




Synthesis of porous polymer-based metal–organic frameworks monolithic hybrid composite for hydrogen storage application

Lerato Y. Molefe^{1,2}, Nicholas M. Musyoka^{1,2,*} , Jianwei Ren¹, Henrietta W. Langmi¹, Patrick G. Ndungu², Robert Dawson³, and Mkhulu Mathe¹

¹HySA Infrastructure Centre of Competence, Energy Centre, Council for Scientific and Industrial Research (CSIR), 627, Meiring Naude Road, Brummeria, Pretoria 0001, South Africa

²Energy Sensors and Multifunctional Nanomaterials Research Group, Department of Applied Chemistry, University of Johannesburg, Doornfontein Campus, Johannesburg, South Africa

³Department of Chemistry, University of Sheffield, Brook Hill, Sheffield, UK

Received: 6 December 2018

Accepted: 16 January 2019

© Springer Science+Business Media, LLC, part of Springer Nature 2019

ABSTRACT

Herein, we report a simple method for the preparation of cross-linked polymer of intrinsic microporosity (PIM-1)/Materials Institute Lavoisier chromium (III) terephthalate [MIL-101(Cr)] monoliths which involves direct impregnation of PIM-1 with MIL-101(Cr) powder by physical mixing in tetrachloroethane solvent. This procedure yields monoliths with high metal–organic framework (MOF) loading weight percentages of up to 80 wt% of MIL-101 powder with little loss of composite mechanical strength. From the nitrogen adsorption isotherms, it was observed that the PIM-1/80 wt% MIL-101(Cr) had good retention of MOF filler surface area and accessibility of its micropores with nearly no pore blocking effects. The hydrogen adsorption was also not far from the estimated hydrogen uptake capacity based on the MIL-101 weight percentage estimation. As a consequence of the highly porous nature of the hybrid material, PIM-1/MIL-101(Cr) composite has been considered as a promising material for inclusion in hybrid hydrogen storage cylinders. Moreover, these composites provided better handling compared to the crystalline powder MOFs without compromising the properties of MOF.

Introduction

The biggest technological challenge hindering the large-scale applications and commercialisation of sustainable hydrogen fuel, especially in mobile

transportation, is due to the absence of efficient, reliable and safe hydrogen (H₂) storage systems [1]. Besides conventional hydrogen liquefaction and highly pressurised hydrogen gas tanks storage methods, which are limited by very high energy

Address correspondence to E-mail: nmusyoka@csir.co.za

consumption for achieving compressed gas or liquid H₂, the physical adsorption of hydrogen on highly porous materials possessing high surface area is emerging as a potential solution for hydrogen storage [2]. Metal–organic frameworks (MOFs), zeolites, porous organic polymers and various carbons have been thoroughly investigated as adsorbents for hydrogen storage applications [2, 3]. The new 2020 United States Department of Energy (US DOE) gravimetric and volumetric storage targets for H₂ are 4.5 wt% and 0.030 kg H₂/L, respectively [4]. These targets are particularly set for a system; that is, calculations of H₂ storage capacity should include pressure containment, cooling systems, valves, etc. Therefore, the storage materials with gravimetric capacities significantly greater than 4.5 wt% are required to achieve these targets. However, the previously mentioned materials are yet to meet all the US DOE 2020 targets set for hydrogen storage materials [2]. Furthermore, for intended practical applications, these materials need to be processed into mechanically stable and easy to handle structures due to the drawbacks associated with their powdery appearance [3, 5]. Therefore, this study aims at investigating novel methods and processes that incorporate powders into structures by producing monoliths of polymer/MOFs composites without adversely compromising the key intrinsic characteristics of the parent materials. To date, there are a very limited number of reports that describe composite materials that meet all the US DOE specified performance necessary for H₂ storage applications. Although powdered MOFs can be processed with various suitable binders, there are limitations in terms of H₂ storage applications; such as, most commercially available inorganic and polymeric binders do not adsorb H₂ and usually block certain pores of the MOF powder materials [5, 6]. One of the current advancements towards processing MOF powders includes their incorporation into polymer films and spheres [7–16]. For instance, Wickenheisser and co-workers fabricated a MOF composite material based on a polymerised resorcinol–formaldehyde xerogel in monolithic form for water adsorption applications [17]. In an extension of their study, they also showed that MOF monoliths can also be shaped by inclusion of Materials Institute Lavoisier chromium (III) terephthalate (MIL-101(Cr)) inside the macropores of poly(2-hydroxyethyl methacrylate) high internal phase emulsion (HIPE) foam. When the

composite was tested for vapour adsorption applications, it showed higher water vapour and methanol uptake capacities compared to pristine HIPE [18].

Recently, it has also been shown that MOFs can be incorporated into three-dimensional (3D) printed polymers [19]. However, in most cases these composites are fabricated as mixed matrix membranes for water and gas adsorption applications. The choice of the polymer used for composites fabrication is an extremely important aspect, and preference is often given to materials which possess reasonable surface area and are able to adsorb hydrogen. This is done so that a polymer matrix does not compromise the hydrogen storage capacity or even other significant properties of the MOF filler material. One of the best porous polymers which exhibit desired properties is polymers of intrinsic microporosity (PIMs) [20, 21]. Although PIMs have previously been applied in hydrogen storage as films, there is a need for development of easy and efficient methods for fabrication of free-standing porous MOF-based composites. In this study, monolithic MOF/polymeric composites were fabricated using the PIM-1 as a matrix for embedding MIL-101(Cr) MOF crystals. Different MOF powder loadings ratios were investigated, and the resulting composites were tested for hydrogen storage application.

Experimental

Materials and chemicals

For the experiments, the following chemicals were used: formic acid (HCOOH, 99.5+%, Sigma-Aldrich), 1,1,2,2-tetrachloroethane (TCE, 98.0+%, Sigma-Aldrich), terephthalic acid (98%, Sigma-Aldrich), chromium chloride hexahydrate (CrCl₃·6H₂O, 99.5+%, Sigma-Aldrich), tetrafluoroterephthalonitrile (C₆F₄-1,4-(CN)₂, 99%, Sigma-Aldrich), 5,5',6,6'-tetrahydroxy-3,3',3',3'-tetramethyl-1,1'-spirobisindane (C₂₁H₂₄O₄, Sigma-Aldrich), potassium carbonate (K₂CO₃), N,N-dimethylformamide (DMF, 99.8%, Sigma-Aldrich), chloroform (CHCl₃) and deionised water. These chemicals were purchased and used without additional purification. Nitrogen (N₂) and hydrogen (99.999%) ultra-high purity grade gases were purchased from Afrox Company, South Africa.

Synthesis of MIL-101(Cr) MOF

MIL-101(Cr) MOF was synthesised following the previously described procedure with some minor modifications [22]. In a typical procedure, terephthalic acid (1.66 g) was dissolved in deionised water (45 mL) with the aid of ultrasonication. Chromium chloride hexahydrate (2.66 g) was also dissolved separately in 55 mL of deionised water. Then, a mixture of the two reactants was transferred to the 250 mL Teflon-lined high-pressure autoclave reactor (Berghof, Germany). Formic acid (30.2 mL, 80 eq) was added to the resulting solution, and the contents were heated to 210 °C and maintained at that same temperature for duration of 8 h. After 8 h, the reaction was stopped and left to cool to room temperature. The resulting Cr-MOF precipitate was washed in hot DMF at 80 °C for 3 h and collected by centrifugation. This was followed by another washing in hot ethanol at 60 °C for 24 h. The obtained product was finally dried overnight at 90 °C in a conventional oven.

Synthesis of PIM-1

PIM-1 was synthesised according to the procedure reported by Budd et al. [23]. Briefly, a mixture of precursors; 5.11 g of 5,5',6,6'-tetrahydroxy-3,3',3'-tetramethyl-1,1'-spirobisindane (15×10^{-3} mol), 16.59 g of anhydrous K_2CO_3 (120×10^{-3} mol) and 3.00 g of tetrafluoroterephthalonitrile (15×10^{-3} mol) were added into a 250-mL three-neck round-bottomed flask fitted with a reflux condenser. Then, the resulting synthesis mixture was purged and backfilled with nitrogen for three times, subsequently a 100 mL anhydrous DMF was added. Sooner, a yellow precipitate appeared and the mixture was then subjected to vigorous stirring for 72 h at 65 °C under N_2 . The resulting synthesis mixture was left to cool to room temperature. Thereafter, 300 mL of water was added to the mixture under stirring for another 1 h. The raw solid product was collected by filtration and was dried at 80 °C under vacuum for 2 days. The obtained solid was dissolved in chloroform and reprecipitated up to three times in 800 mL of methanol. The final product was collected and dried under vacuum at 60 °C overnight.

Ex-situ synthesis of the PIM-1/MIL-101(Cr) monolithic composite materials

The direct impregnation of PIM-1 with MIL-101(Cr) powder by physical mixing in tetrachloroethane solvent can readily lead to cross-linked PIM-1/MIL-101(Cr) monolith bodies. This was achieved by preparing separate tetrachloroethane-based solutions of PIM-1 and suspension of various loadings of pre-dried MIL-101(Cr) powder (40, 60 and 80 wt%). The solutions were mixed with each other in a 20 mL cylindrical glass vial and further subjected to a vigorous magnetic stirring overnight to achieve a desired homogeneous mixture of PIM-1/MIL-101(Cr). The resulting viscous mixture was thereafter heated to 150 °C to evaporate the solvent and a monolith was obtained. PIM-1 has good solubility in tetrachloroethane such that it helped in forming a homogenous mixture with MIL-101 and readily produced monolithic gels.

The following formula was used to calculate the wt% of MOF in PIM-1/MIL-101(Cr) composite:

$$\text{wt}\% = \frac{M_{\text{MIL-101}}}{M_{\text{MIL-101}} + M_{\text{PIM-1}}} \times 100$$

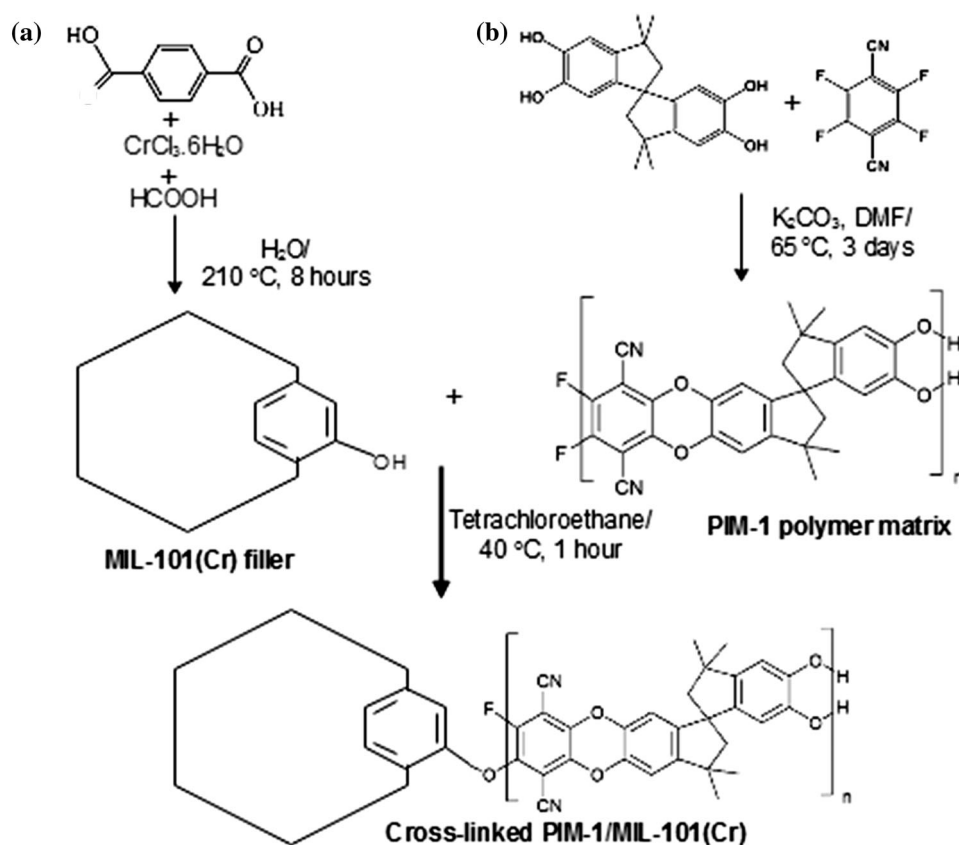
where $M_{\text{MIL-101}}$ and $M_{\text{PIM-1}}$ represent the masses of MIL-101 and PIM-1 powders, respectively.

A summary of the procedure used for synthesis of pristine PIM-1 and MIL-101(Cr) together with the MOF composite is shown in Scheme 1 below.

Sample characterisation

The powder X-ray diffractometer (PANalytical X'Pert Pro), coupled to a Pixcel detector (Cu-K_α radiation $\lambda = 0.154$ nm), was used to obtain powder X-ray diffraction (PXRD) patterns at scanning rate of 2° min^{-1} . The samples were measured at room temperature. The morphological analysis of the obtained samples was conducted using focused ion beam scanning electron microscope (Carl Zeiss Auriga Cobra). TGA/SDTA 851^e instrument (Mettler Toledo) was used to carry out the thermogravimetric analysis (TGA), in a temperature range of 46–1000 °C and heating rate of $10^\circ \text{ C min}^{-1}$ under air (60 mL min^{-1}) and nitrogen flow (40 mL min^{-1}) as a balance gas. The nitrogen and hydrogen sorption (up to 1 bar) measurements were obtained from a Micrometrics ASAP 2020 HD analyser at 77 K. The specific surface areas by Brunauer–Emmett–Teller (BET) theory and

Scheme 1 Schematic procedure to prepare molecular cross-linked PIM-1/MIL-101(Cr) monoliths.



pore size distributions (PSDs) were obtained from the nitrogen physisorption isotherms. Before any gas sorption experiment, the samples were outgassed in the degassing port under vacuum (down to 10^{-7} bar) for at least 8 h at 200 °C for removal of moisture or other volatile contaminants.

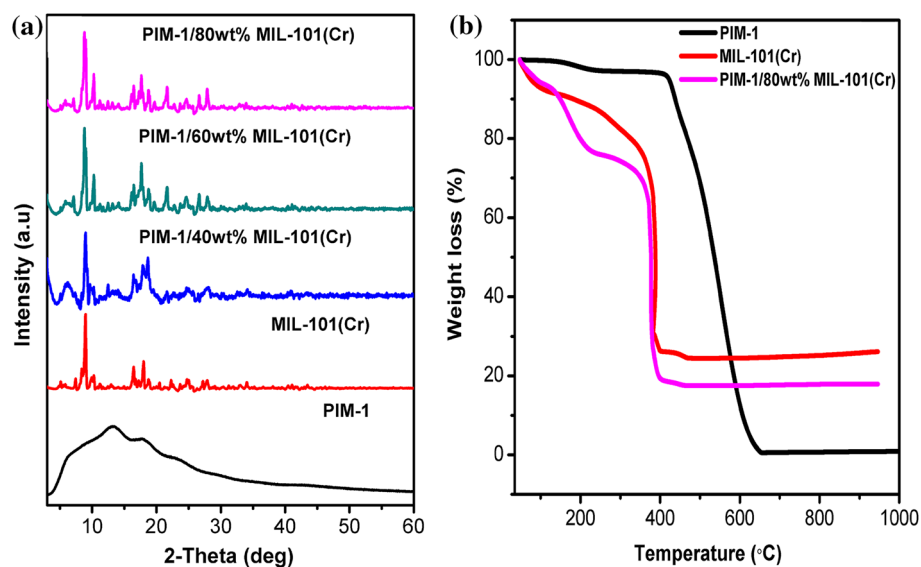
Results and discussion

PXRD plots of PIM-1/MIL-101(Cr) composite materials (Fig. 1a) demonstrate unchanged crystalline phase of as-synthesised MIL-101 [with all major characteristic peaks of MIL-101(Cr) at around $2\theta = 5.2^\circ$, 8.5° and 9.1°] as earlier reported [21]. The broad peak observed for the PIM-1 sample depicts its amorphous nature. It could also be observed that as the quantity of MIL-101(Cr) filler was increased in the hybrid materials there was some corresponding increase in the intensity of the main characteristic peaks of the MOF. Simultaneously, there was a reduction in the amorphous hump that was related to the PIM-1 material. The TGA curves (Fig. 1b) of both pristine PIM-1 and MIL-101(Cr) materials compare

well with previous reports [23, 24], showing PIM-1 and MIL-101(Cr) to be stable up to ~ 430 °C and ~ 350 °C, respectively. The high thermal stability observed for PIM-1 is attributed to intense dipolar interactions of the cyano ($-\text{C}\equiv\text{N}$) functional groups in the polymer chains [25]. The first continuous weight loss step (~ 150 – 200 °C) for the MOF and PIM-1/80 wt% MIL-101(Cr) can be ascribed to the evaporation of DMF and water absorbed in the pores of the MOF. However, the observable difference at the lower temperatures [where PIM-1/80 wt% MIL-101(Cr) suffered an excessive mass loss compared to MIL-101(Cr)] could possibly be due to evaporation of residual tetrachloroethane solvent. The mass loss observed at around 350 – 470 °C for the MIL-101(Cr) can be assigned to the disintegration of the MOF structure [22].

Scanning electron micrographs in Fig. 2a, b show the porous nature of the PIM-1 sample and the octahedral shaped crystals for the MOF sample. Even though PIM-1 powder is a microporous material, the observed porosity in the macroscale together with the high roughness can be attributed to the evaporation of the solvent during the synthesis process. Polak-

Figure 1 **a** Stacked PXRD patterns and **b** TGA profiles of PIM-1, MIL-101(Cr) and PIM-1/MIL-101(Cr) composites samples.



Krašna et al. [21] had also attributed the chaotic nature of the solvent evaporation process as the main responsible factor in the non-uniform distribution of the observed macropores. In the PIM-1/MOF

composite samples (Fig. 1c–e), the respective morphologies of pristine materials after the physical mixing were maintained. Furthermore, it was observed that most of the MOF particles were well

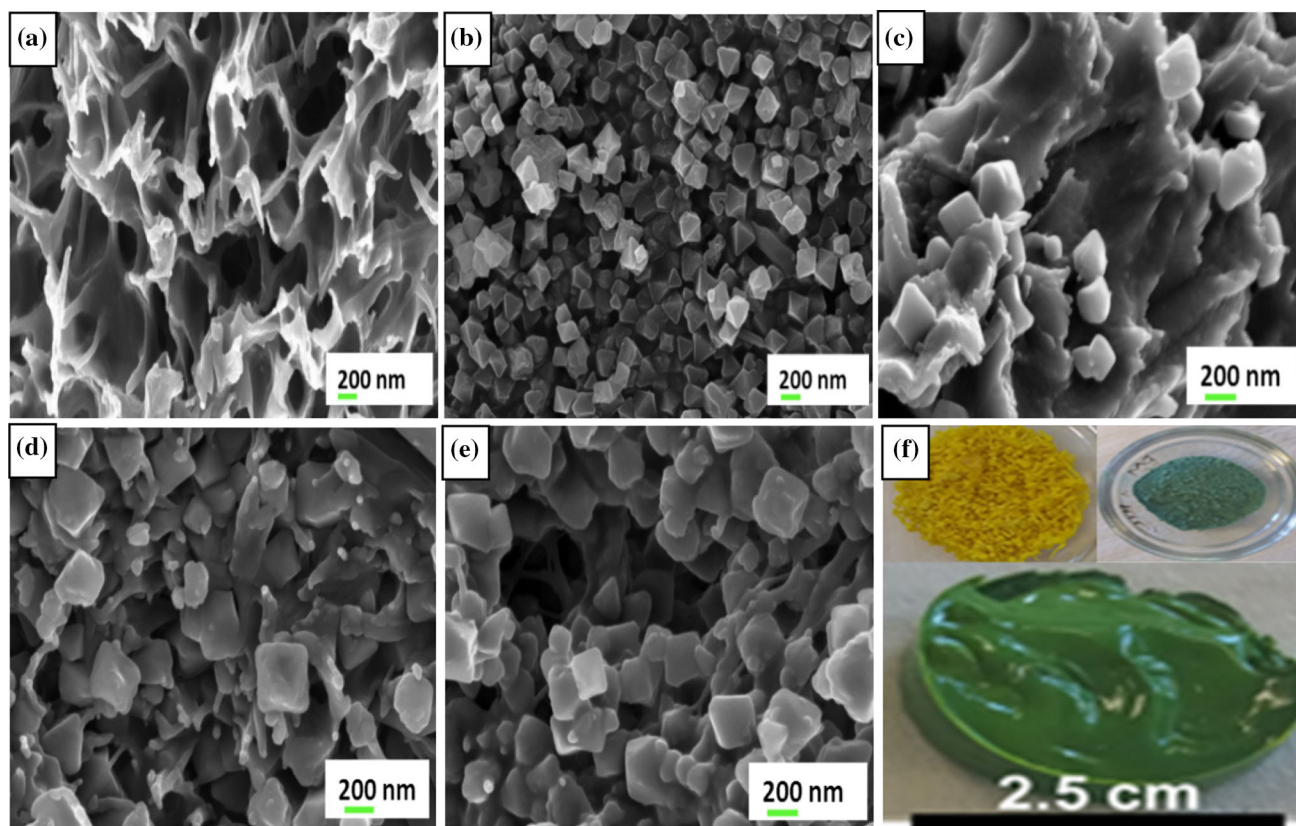


Figure 2 High-resolution scanning electron micrographs of **a** pristine PIM-1 and **b** MIL-101(Cr) and respective MIL-101(Cr) embedded PIM-1 composite with various MIL-101(Cr)

loadings of **c** 40 wt%, **d** 60 wt% and **e** 80 wt% and **f** pictures of pristine PIM-1 powder, MIL-101(Cr) powder and PIM-1/MIL-101(Cr) monolith.

dispersed in PIM-1 matrix although some agglomeration had been observed at high 80 wt% MOF loading. The mechanical strength of the composite was observed to decrease as the MOF loading was increased. The samples with loading above 80 wt% of MIL-101 (Cr) were observed to crumble easily and for future experiments this will be avoided by adding a surface modifier to improve the compatibility between PIM-1 and the MIL-101(Cr).

The nitrogen sorption isotherms for PIM-1 and MIL-101(Cr) presented in Fig. 3a share similar patterns with those previously reported, where PIM-1 isotherm revealed both Type I for microporosity and Type IV for mesoporosity indicating hierarchical porosity behaviour [26]. The presence of a relatively large hysteresis was also reported by Polak-Krašna et al. [21] and was attributed to occur either due to the presence of narrow pore channels or possible pore swelling. On the other hand, the N₂ sorption isotherms for MIL-101(Cr) and composites materials displayed Type IV behaviour with smaller hysteresis loop which indicates that samples were more microporous than mesoporous. This is corroborated by their pore size distribution curves based on density functional theory (DFT) model presented in Fig. 3b and as well as the data shown in Table 1. From the DFT pore size distribution, the 40 and 60 wt% composites showed a broad multi-modal pore size distribution at 1.1, 1.7, 2.3 and 3.5 nm, whereas

for the 80 wt% composite, pore sizes displayed some narrow distribution almost similar to that of MIL-101(Cr) centred at 1.1–2.1 nm. In summary, the PSD curves confirmed the increasing micropore characteristics of composites as the MIL-101(Cr) content increased.

The surface area and total pore volume of hybrid materials were found to increase proportionally to the weight per cent loading of MIL-101 as displayed in Table 1. However, the actual measured surface area of PIM-1/80 wt% MIL-101(Cr) is slightly higher than estimated from a rule of mixtures calculations as shown in Eq. 1.

$$\begin{aligned} \text{Surface area (composite)} = & W_{\text{PIM-1}} \\ & \times \text{surface area(PIM-1)} \\ & + W_{\text{MIL-101}} \\ & \times \text{surface area(MIL-101)} \end{aligned} \quad (1)$$

wherein the property of a composite is a weighed mean of the characteristics of its individual components, and where $W_{\text{MIL-101}}$ and $W_{\text{PIM-1}}$ are the weight fractions of MIL-101 and PIM-1, respectively, such that, $W_{\text{PIM-1}} + W_{\text{MIL-101}} = 1$.

It is noteworthy that the measured specific surface area of pristine PIM-1 increased from 784 to 2347 m² g⁻¹ upon preparation of the PIM-1/MOF composite, which represents a significant threefold increase. The anomaly observed in the measured versus predicted surface areas of PIM-1/80 wt% MIL-101(Cr) can be due to the possibility of an increased external surface area which led to some exposed MOF crystal surface when the sample was almost saturated due to the high MOF loading. There is also a possibility that the earlier observed mesoporosity in the pristine powder PIM-1 (SEM images) due to reprecipitation had been eliminated and thus amplifying the intrinsic microporosity which interacted synergistically with the MOF physical properties. The inability to obtain complete N₂ desorption isotherms was due to the impractical long times that the samples took to achieve equilibration in the low-pressure ranges. Similar observations were also reported earlier [21].

The H₂ storage capacities (Fig. 4) were observed to follow a similar trend to the specific surface areas, where the H₂ uptake increased from 1.02 wt% for pristine PIM-1 to 1.73 wt% in PIM-1/80 wt% MIL-101(Cr). This was expected as the H₂ adsorption capacity and specific surface area are directly

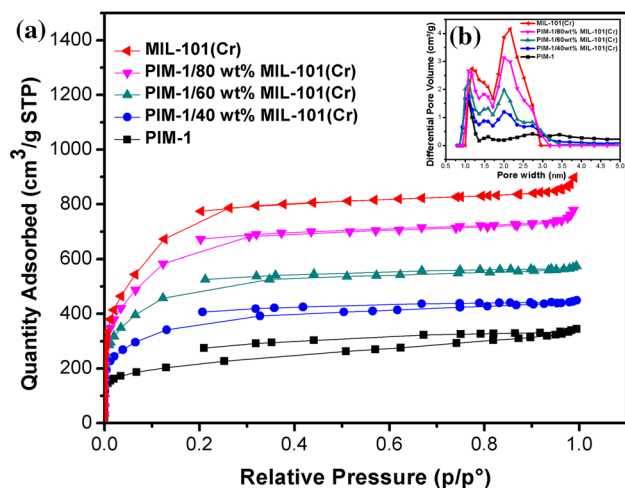


Figure 3 a N₂ adsorption–desorption isotherms of pristine and composites materials at 77 K and corresponding b Density Functional Theory (DFT) pore size distribution (insert) of pristine MIL-101(Cr) MOF and their respective PIM-1 composites.

Table 1 Physical properties of pristine and composites materials

Sample	Measured BET SSA (m ² g ⁻¹) ^a	Estimated BET SSA (m ² g ⁻¹) ^b	Micropore area (m ² g ⁻¹) ^c	Pore size (nm) ^d	Total pore vol. (cm ³ g ⁻¹) ^e	H ₂ uptake (wt%) ^f
Pristine MIL-101(Cr)	2720	—	2636	1.2–2.2	1.39	1.76
PIM-1/80 wt% MIL-101(Cr)	2347	2333	2290	1.1–2.1	1.20	1.73
PIM-1/60 wt% MIL-101(Cr)	1821	1946	1781	1.1–2.7	0.89	1.50
PIM-1/40 wt% MIL-101(Cr)	1331	1558	1273	1.1–3.6	0.70	1.32
Pristine PIM-1	784	—	693	1.1–3.5	0.53	1.02

^aBET surface area measured from N₂ adsorption isotherms at 77 K

^bBET surface area calculated as the sum of the mass-weighted surface areas of the MOF and PIM-1 from this formula: $\text{BET (estimated)} = \frac{\text{wt\% of MIL-101}}{100} \times 2720 \text{ m}^2 \text{ g}^{-1} + \frac{\text{wt\% of PIM-1}}{100} \times 784 \text{ m}^2 \text{ g}^{-1}$

^cFrom *t*-plot

^dPore size determined by DFT analysis

^eTotal pore volume determined from H–K analysis by uptake at $p/p^\circ \sim 0.99$

^fHydrogen adsorbed at 77 K and 1 bar

correlated [3, 27]. Unlike other polymeric materials that have been used to shape MOFs [6], the use of PIM-1 clearly shows advantages due to the fact that the obtained hydrogen storage capacity for the PIM-1/MOF is almost similar to that of the MOF. Furthermore, the shaping of the MOF through composite formation with PIM-1 leads to better handling while simultaneously is retaining the MOF's hydrogen storage capacity. Importantly, all the H₂ adsorption isotherms indicated a sharp rise at low pressure up to 1 bar without reaching a point of saturation (plateau).

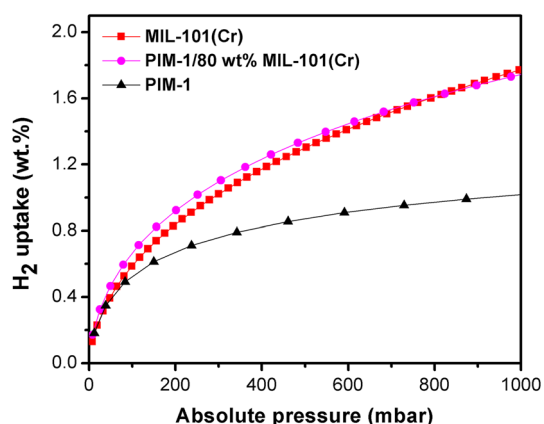


Figure 4 H₂ adsorption isotherms of pristine and composites materials at 77 K and 1 bar.

Consequently, higher hydrogen uptake would be expected at pressures higher than 1 bar [28].

Conclusion

We successfully fabricated self-standing PIM-1/MOF composite monoliths containing various loadings of MIL-101(Cr) filler. The obtained composites exhibited enhanced specific surface areas coupled with improved hydrogen uptake capacities with the highest MOF loading (80 wt%) showing the best properties. Based on the adaptation of the estimation formula used for calculating estimated BET surface area, the obtained H₂ uptake capacity of the composite derived from 40 and 60 wt% loadings of MIL-101(Cr) was found to be close to the estimated values. However, for 80 wt% loading, a hydrogen uptake of 1.73 wt% was obtained which is 7.5% higher than the estimated value (1.61 wt%). The use of PIM-1, as a binder, proved advantageous since it did not show any signs of MIL-101(Cr) micropore blockage. The work presented here contributes towards the ongoing efforts to improve the hydrogen storage conditions for future application in light-duty vehicles by demonstrating that MIL-101(Cr) can easily be embedded into PIM-1 for better handling while maintaining its functionality. Future work will

include mechanical strength experiments, high-pressure H₂ uptake measurements, kinetics and heat of adsorption studies.

Acknowledgements

The authors acknowledge financial support from the Department of Science and Technology (DST) of South Africa towards HySA Infrastructure (Grant No. EIMH01X), National Research Foundation (NRF) for NM Musyoka's Y-rated researcher development grant (Grant No. EIMH05X) and the Royal Society—DFID Africa Capacity Building Initiative Programme Grant (Grant No. AQ150029).

Compliance with ethical standards

Conflict of interest There are no conflicts of interest to declare.

References

- [1] Schlapbach L, Züttel A (2011) Hydrogen-storage materials for mobile applications. *Materials for sustainable energy: a collection of peer-reviewed research and review articles from Nature Publishing Group* 265–270
- [2] Lim KL, Kazemian H, Yaakob Z, Daud WW (2010) Solid-state materials and methods for hydrogen storage: a critical review. *Chem Eng Technol* 33:213–226
- [3] Ren J, Langmi HW, North BC, Mathe M (2015) Review on processing of metal–organic framework (MOF) materials towards system integration for hydrogen storage. *Int J Energy Res* 39:607–620
- [4] U.S. Department of Energy (2018) DOE Technical targets for onboard hydrogen storage for light-duty vehicles. <https://www.energy.gov/eere/fuelcells/doe-technical-targets-onboard-hydrogen-storage-light-duty-vehicles>. Accessed 19 July 2018
- [5] Ren J, Musyoka NM, Langmi HW, Swartbooi A, North BC, Mathe M (2015) A more efficient way to shape metal–organic framework (MOF) powder materials for hydrogen storage applications. *Int J Hydrogen Energy* 40:4617–4622
- [6] Ren J, Dyosiba X, Musyoka NM, Langmi HW, Mathe M, Liao S (2017) Review on the current practices and efforts towards pilot-scale production of metal-organic frameworks (MOFs). *Coord Chem Rev* 352:187–219
- [7] Huo J, Marcello M, Garai A, Bradshaw D (2013) MOF-polymer composite microcapsules derived from pickering emulsions. *Adv Mater* 25:2717–2722
- [8] Zomoza B, Tellez C, Coronas J, Gascon J, Kapteijn F (2013) Metal organic framework based mixed matrix membranes: an increasingly important field of research with a large application potential. *Microporous Mesoporous Mater* 166:67–78
- [9] Zhu QL, Xu Q (2014) Metal-organic framework composites. *Chem Soc Rev* 43:5468–5512
- [10] Denny MS, Cohen SM (2015) In situ modification of metal-organic frameworks in mixed-matrix membranes. *Angew Chem Int Ed* 54:9029–9032
- [11] Seoane B, Coronas J, Gascon I, Benavides ME, Karvan O, Caro J, Kapteijn F, Gascon J (2015) Metal–organic framework based mixed matrix membranes: a solution for highly efficient CO₂ capture? *Chem Soc Rev* 44:2421–2454
- [12] Zhang ZJ, Nguyen HTH, Miller SA, Cohen SM (2015) PolyMOFs: a class of interconvertible polymer-metal–organic-framework hybrid materials. *Angew Chem Int Ed* 54:6152–6157
- [13] Kubica P, Wolinska-Grabczyk A, Grabiec E, Libera M, Wojtyniak M, Czajkowska S, Domański M (2016) Gas transport through mixed matrix membranes composed of polysulfone and copper terephthalate particles. *Microporous Mesoporous Mater* 235:120–134
- [14] DeCoste JB, Denny MS, Peterson GW, Mahle JJ, Cohen SM (2016) Enhanced aging properties of HKUST-1 in hydrophobic mixed-matrix membranes for ammonia adsorption. *Chem Sci* 7:2711–2716
- [15] Ling RJ, Ge L, Diao H, Rudolph V, Zhu ZH (2016) Ionic liquids as the MOFs/polymer interfacial binder for efficient membrane separation. *ACS Appl Mater Interfaces* 8:32041–32049
- [16] Zhang ZJ, Nguyen HTH, Miller SA, Ploskonka AM, DeCoste JB, Cohen SM (2016) Polymer-metal–organic frameworks (polyMOFs) as water tolerant materials for selective carbon dioxide separations. *J Am Chem Soc* 138:920–925
- [17] Wickenheisser M, Herbst A, Tannert R, Milow B, Janiak C (2015) Hierarchical MOF-xerogel monolith composites from embedding MIL-100 (Fe, Cr) and MIL-101 (Cr) in resorcinol-formaldehyde xerogels for water adsorption applications. *Microporous Mesoporous Mater* 215:143–153
- [18] Wickenheisser M, Janiak C (2015) Hierarchical embedding of micro-mesoporous MIL-101 (Cr) in macroporous poly (2-hydroxyethyl methacrylate) high internal phase emulsions with monolithic shape for vapor adsorption applications. *Microporous Mesoporous Mater* 204:242–250
- [19] Channell MN, Sefa M, Fedchak JA, Scherschligt J, Miller AE, Ahmed Z, Hartings MR (2017) Toward 3D printed hydrogen storage materials made with ABS-MOF composites. *Polym Adv Technol* 1–7

- [20] Rochat S, Polak-Kraśna K, Tian M, Holyfield LT, Mays TJ, Bowen CR, Burrows AD (2017) Hydrogen storage in polymer-based processable microporous composites. *J Mater Chem A* 5:18752–18761
- [21] Polak-Kraśna K, Dawson R, Holyfield LT, Bowen CR, Burrows AD, Mays TJ (2017) Mechanical characterisation of polymer of intrinsic microporosity PIM-1 for hydrogen storage applications. *J Mater Sci* 52:3862–3875. <https://doi.org/10.1007/s10853-016-0647-4>
- [22] Ren J, Musyoka NM, Langmi HW, Segakweng T, North BC, Mathe M, Kang X (2014) Modulated synthesis of chromium-based metal-organic framework (MIL-101) with enhanced hydrogen uptake. *Int J Hydrogen Energy* 39:12018–12023
- [23] Budd PM, Elabas ES, Ghanem BS, Makhseed S, McKeown NB, Msayib KJ, Tattershall CE, Wang D (2004) Solution-processed, organophilic membrane derived from a polymer of intrinsic microporosity. *Adv Mater* 16:456–459
- [24] Wu X, Liu W, Wu H, Zong X, Yang L, Wu Y, Ren Y, Shi C, Wang S, Jiang Z (2018) Nanoporous ZIF-67 embedded polymers of intrinsic microporosity membranes with enhanced gas separation performance. *J Membr Sci* 548:309–318
- [25] Yang JF, Zhao Q, Li JP, Dong JX (2010) Synthesis of metal-organic framework MIL-101 in TMAOH-Cr(NO₃)₃-H₂BDC-H₂O and its hydrogen-storage behaviour. *Microporous Mesoporous Mater* 130:174–179
- [26] Du N, Robertson GP, Song J, Pinnau I, Thomas S, Guiver MD (2008) Polymers of intrinsic microporosity containing trifluoromethyl and phenylsulfone groups as materials for membrane gas separation. *Macromolecules* 41:9656–9662
- [27] Broom DP, Webb CJ, Hurst KE, Parilla PA, Gennett T, Brown CM, Zacharia R, Tylianakis E, Klontzas E, Froudakis GE, Steriotis TA (2016) Outlook and challenges for hydrogen storage in nanoporous materials. *Appl Phys A* 122:151–171
- [28] Ren J, Musyoka NM, Langmi HW, North BC, Mathe M, Kang X (2014) Fabrication of core-shell MIL-101(Cr)@UiO-66(Zr) nanocrystals for hydrogen storage. *Int J Hydrogen Energy* 39:14912–14917